PROCEEDINGS OF SCIENCE

Mu2e: Probing the Frontiers of Physics Using Muons

E. Craig Dukes[a,1,*]

[a] *University of Virginia, Charlottesville, VA, USA*

E-mail: ecd3m@virginia.edu

The absence of any signature for new physics beyond the standard model at the Large Hadron Collider has left the field of elementary particle physics in a quandary. We know there is new physics out there: where best to look for it? Searches for certain rare processes provide ultra-sensitive probes for new physics and can reach mass scales unobtainable by any conceivable accelerator, present or imagined. We describe such an experiment, Mu2e, that intends to use a novel technique to search for new physics through lepton flavor violation in muon decays with a sensitivity of a factor of 10,000 over existing limits.

25th International Spin Physics Symposium (SPIN 2023)
24-29 September 2023
Durham, NC, USA

[1] For the Mu2e Collaboration: https://mu2e.fnal.gov/mu2e_collaboration_list_2024.shtml.
[*] Speaker

PoS(SPIN2023)122

1. Introduction

The standard model of particle physics has successfully described nature at its most fundamental level for many decades. We know, however, that it is incomplete. For example, it does not describe the origin of the asymmetry between matter and antimatter in the universe. Nor does it shed any light on the nature of dark matter or dark energy. Non-zero neutrino masses must be put in by hand. And there is no accepted quantum theory of gravity.

Hence, in recent years the impetus for searches for physics beyond the standard model has grown, and occasionally hints of such physics have appeared, only to disappear with better measurements. We are left with a standard model that explains almost everything we measure in accelerator-based experiments, but does not explain the very gross features we unambiguously observe in the universe.

Since theory provides little guidance for the experimentalist of where to look for this new physics, broad searches are needed. One of the best probes of physics beyond the standard model is the search for charged lepton flavor violation (CLFV). As has been pointed out by many authors, e.g. Ref [1], such searches probe a large array of new physics models with good sensitivity. CLFV searches have a long history that started in 1947, a decade after the discovery of the muon [2]. As displayed in Fig. 1, which shows only searches for CLFV in muons, impressive advances in sensitivity were made until the 1990s. However, a new generation of experiments are being mounted with much improved sensitivities. We describe one of them, Mu2e [3], in this article.

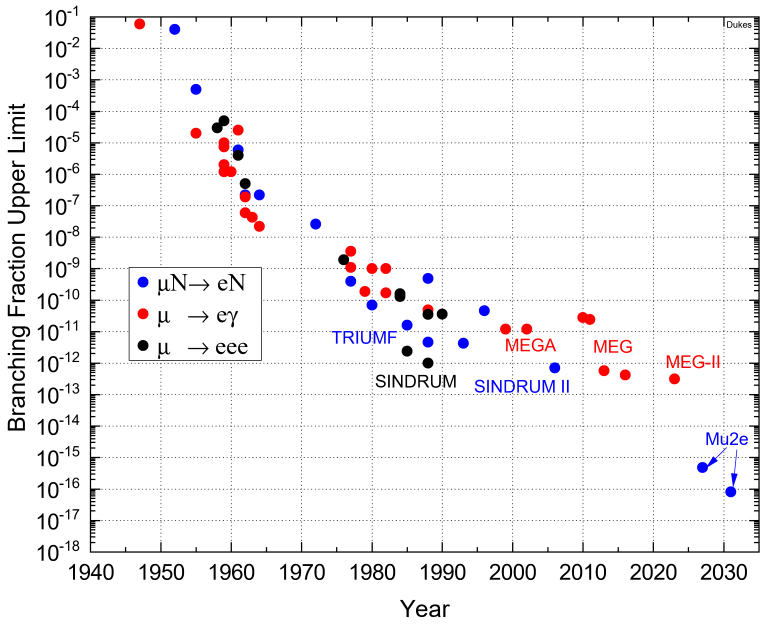

Figure 1: History of searches for CLFV in muons, including the projected Run 1 and Run 2 sensitivities of the Mu2e experiment.

2. Experimental Technique

Mu2e intends to search for the conversion of a negatively charged muon into an electron in the presence of an aluminum nucleus: $\mu^-\mathrm{Al} \rightarrow e^-\mathrm{Al}$. In the standard model this process is

forbidden: in the extended standard model (Fig. 2) with non-zero neutrino masses, it proceeds at the experimentally unobservable rate of $\sim 10^{-52}$. Hence, any observation of this process would be unambiguous evidence of new physics (e.g., SUSY as shown in Fig. 3).

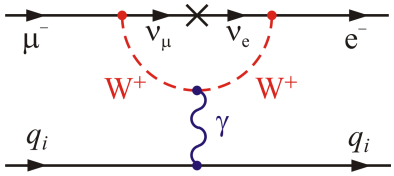

Figure 2: $\mu^- N \rightarrow e^- N$ in the extended standard model with non-zero neutrino masses.

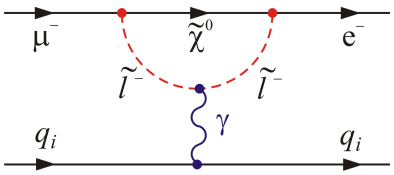

Figure 3: $\mu^- N \rightarrow e^- N$ mediated by a SUSY process.

To search for $\mu^- N \rightarrow e^- N$ an intense, low-energy muon beam is needed. The muons are stopped in a thin target where they rapidly $O\left(10^{-13}\,\mathrm{s}\right)$ cascade down to the 1S state. The muon circles the nucleus until one of two processes is likely to occur: (1) the muon is captured by the nucleus: $\mu^- N_{\mathrm{A,Z}} \rightarrow \nu_\mu N_{\mathrm{A,Z-1}}$, producing an unobservable neutrino, or (2) the muon decays in orbit $\mu^- N_{\mathrm{A,Z}} \rightarrow e^- \nu_\mu \overline{\nu}_e N_{\mathrm{A,Z}}$. Mu2e is searching for a third process: the coherent direct conversion of the muon into an electron: $\mu^- N \rightarrow e^- N$. The signature for this third process is the emission of a isolated, delayed electron with an energy given by essentially the rest-mass energy of the muon. In the aluminum stopping target to be used by Mu2e, the delay is on average 864 ns, and the electron energy is 104.97 MeV.[1] The large delay is important as the intense muon beam, with its unavoidable attendant other charged particles, produces an intense prompt flash of secondary particles in the apparatus that takes several hundreds nanoseconds to mitigate to an acceptable level.

The goal of Mu2e since its inception has been to achieve a single event sensitivity of $O\left(10^{-18}\right)$. In order to do so a new high-intensity, low-energy muon beam has to be built. This is done by taking 8 GeV proton batches from the Fermilab Booster accelerator, using the Recycler Ring to rebunch each batch into four bunches. Each bunch is individually transferred to the Delivery Ring (formerly the antiproton Debuncher), where they are slow extracted in a spill of 1.333s (1.400s) duration for Run 1 (Run 2). The protons are delivered to the Mu2e production target (Fig. 4) in pulses. called microbunches, of $\sim 16 \times 10^6$ ($\sim 39 \times 10^6$) protons for Run 1 (Run 2), each separated by 1695 ns.

The muon beam is then produced by a scheme first proposed by the MELC collaboration [4] and shown schematically in Fig. 4 below. There are three large solenoidal magnets: the production, transport, and detector solenoids, with the highest magnetic field of 4.6 T at the far end of the production solenoid, followed by an ever decreasing field, with the smallest value being 1.0 T, at the end of the detector solenoid. The field gradient serves to push charged particles to the downstream end of the detector solenoid, eliminating trapped charged particles. Charged pions from the 8 GeV proton beam incident on the production target decay into muons that are captured in the field of the production solenoid. Backward-going muons, and muons reflected backwards in the gradient field of the production solenoid, enter the transport solenoid, whose S-shape serves two purposes. It deflects the charged muons in opposite directions vertically, allowing a collimator at the center to pass only negative muons. It also prevents neutral particles from the production target reaching the stopping target, where they can produce unwanted backgrounds.

[1] The energy is slightly less than the rest mass of the muon due to the small recoil energy of the much more massive nucleus and by the small binding energy of the nucleus.

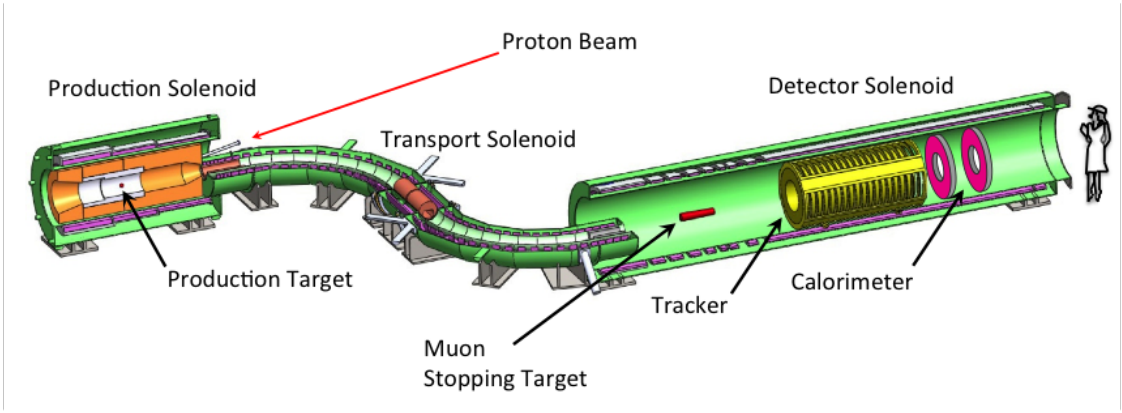

Figure 4: The Mu2e apparatus (with the cosmic ray veto detector removed).

3. The Apparatus

The spectrometer, shown in Fig. 4, consists of the stopping target, a tracker, and an electromagnetic calorimeter. Not shown in the figure is the cosmic ray veto that surrounds the detector solenoid and part of the transport solenoid, the stopping target monitor downstream of the detector solenoid, which is used to measure the rate of muon captures in the stropping target, and the extinction monitor beyond the end of the production solenoid, which is used to measure the rate of protons that come in between pulses. The tracker and the calorimeter must operate in a vacuum in order to reduce multiple scattering of the low-energy conversion electrons. They must also handle the intense beam flash produced from the proton bunch every 1695 ns, as well as the intense number of muon decay-in-orbit electrons emanating from the stopping target during the live gate time. The spectrometer is turned off during and just after the beam flash, after which data is taken for some 1010 ns before the next pulse (Fig. 5).

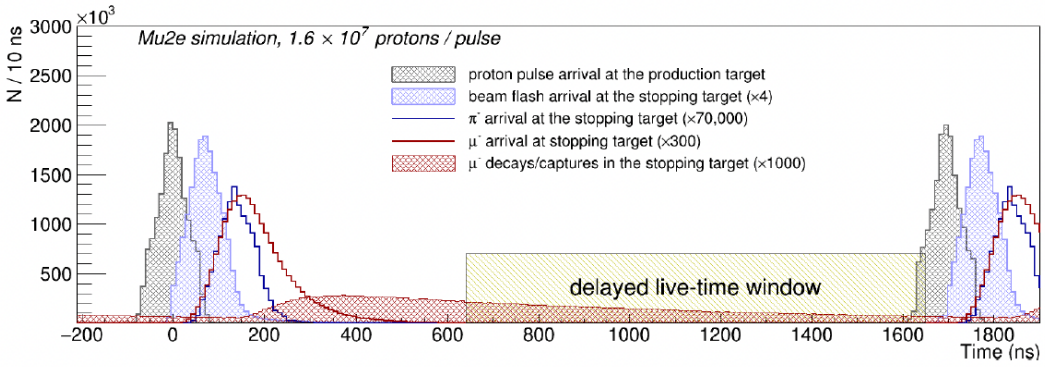

Figure 5: The muon beam timeline. After each proton pulse is a large beam flash of particles in the detector elements while the spectrometer is turned off. Following the beam flash by several hundred nanoseconds is the live window of 1010 ns duration during which data is taken.

Roughly half of the beam muons are stopped in an array of 37, 0.1 mm thick aluminum foils, spaced out to minimize the energy loss by the conversion elections. Holes in the stopping-target foils

allow the core of the prompt beam to pass through without interactions, minimizing the radiation load to the tracker and the electromagnetic calorimeter.

Downstream of the stopping target is the straw tracker. The tracker must have excellent momentum resolution in order to discriminate the 104.97 MeV conversion electrons from the copious number of lower-energy electrons from the muon decay-in-orbit process. Although the vast majority of those background muon decay-in-orbit electrons have half the momentum of the conversion electrons, the tail of the muon decay-in-orbit spectrum creeps up to the signal region, as is shown in Fig. 6. The tracker must also operate in a vacuum and be sufficiently thin in order to reduce scattering and minimize energy loss of the low-energy conversion electrons.

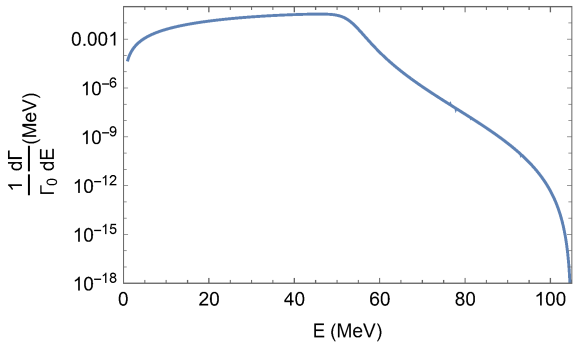

Figure 6: The muon decay-in-orbit spectrum for aluminum [5].

The tracker is composed of 20,736, 5-mm-diameter, 15-μm-thick, gold-over-aluminum coated, Mylar straws, arranged in a octagonal geometry around the axis of the detector solenoid. They are grouped in 36 double-layer planes (Fig. 8). Each straw is read out on both ends; the working gas is a 80:20 $ArCO_2$ mixture. The straws range in lengths from 330 mm to 1170 mm.

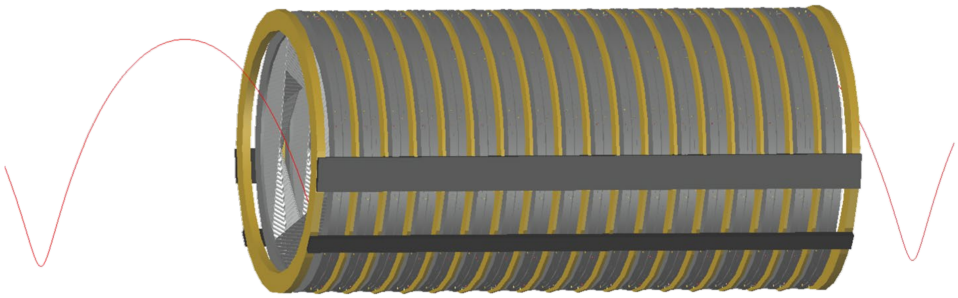

Figure 7: Isometric view of the straw tracker showing a 105 MeV/c electronic incident upon it. The tracker is approximately 3 m long with an outer radius of 0.85 m.

Simulation studies show an excellent momentum resolution at the conversion electron energy, of order 0.14 MeV/c in the central part of the distribution, assuming no target energy loss. Most importantly, as shown in Fig. 9, there is a negligible high-side tail in the momentum measurement. This is vital in order to prevent the copious decay-in-orbit electrons' momenta from migrating into the conversion electron signal region. The acceptance of the tracker for conversion electrons is greater than 20%, that for decay-in-orbit electrons is less than 10^{-3}.

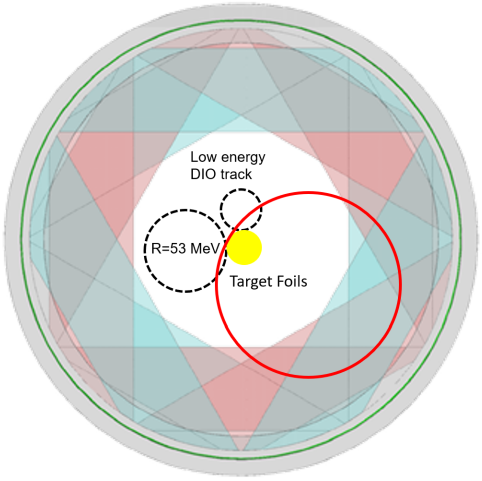

Figure 8: Beams-eye view of the straw tracker. The straws are arranged so that the vast majority of the decay-in-orbit muons (black) do not make it to the 0.38 m inner radius, whereas electrons with a $p_T > 90\,\text{MeV}/c$ and an angle of $90° \pm 30°$ relative to the solenoid axis have their helix trajectories well measured.

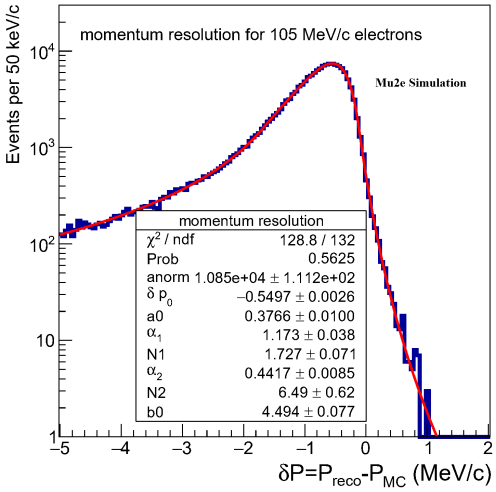

Figure 9: Tracker momentum resolution for 105 MeV/c electrons.

Downstream of the straw tracker are two electromagnetic calorimeter disks, separated by one-half of the helix wavelength the conversion electrons make (Fig. 10). Each disk consists of 674 un-doped CsI crystals of $34\times34\times200\,\text{mm}^3$ size, each read out by two UV-extended silicon photomultiplier arrays. The purpose of the calorimeter is to provide a trigger, seed the track reconstruction algorithm, and provide sufficient particle identification to reject muons that are reconstructed as electrons in the straw tracker. The crystals and their electronics have been designed to survive a dose of 90 krad and a neutron fluence of $3\times10^{12}\,\text{n/cm}^2$. Like the tracker, it must operate in a vacuum. Studies show that the calorimeter can reject muons by a factor of over 200 through its excellent energy and time resolutions: see Fig. 11 and Fig. 12 below.

Zero-suppressed data streamed from the straw tracker and the electromagnetic calorimeter are fed into a farm of processors in the counting room that provide a software trigger used to select the microbunches of interest during the 1.333 s (1.400 s) long Run 1 (Run 2) spill that are to be stored on tape. This trigger is used to select the data from the cosmic ray veto (described below) that is to be read out.

4. Backgrounds

For any sensitive search experiment it is vital to keep backgrounds in check, if at all possible to less than one event. Hence, the apparatus has been designed to minimize backgrounds while keeping the signal efficiency high. An enormous simulation effort has been done to estimate the various backgrounds: see Ref. [6] for details. The backgrounds come in three types: (1) stopped-muon-induced backgrounds; (2) beam related backgrounds; and (3) time dependent backgrounds.

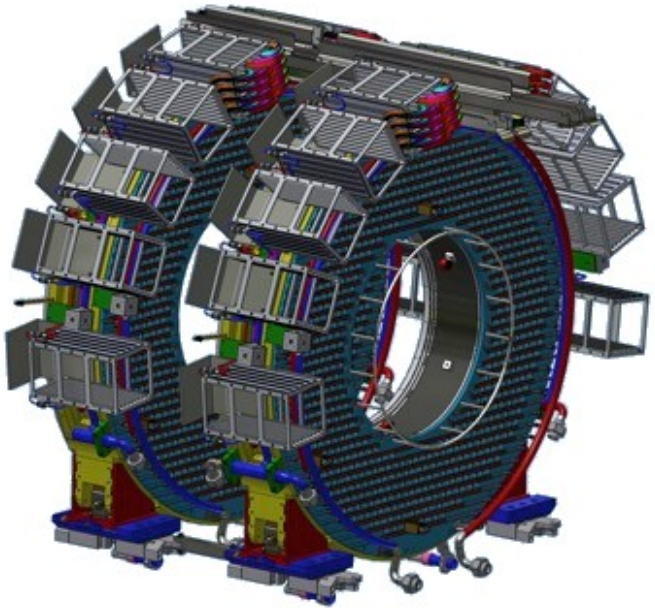

Figure 10: The two electromagnetic calorimeter disks.

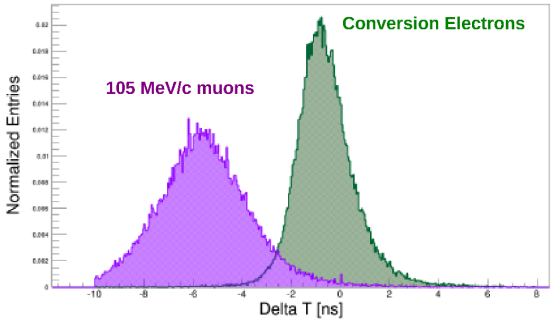

Figure 11: Time difference between 105 MeV/c muons and conversion electrons as measured by the electromagnetic calorimeter.

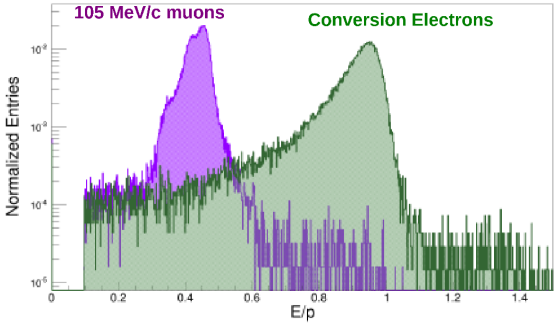

Figure 12: E/p for 105 MeV/c muons and conversion electrons.

The largest stopped muon induced background is the huge muon decay-in-orbit rate: $\mu^- \mathrm{Al} \rightarrow e^- \nu_\mu \overline{\nu}_e \mathrm{Al}$. Although most of the electrons from this process do not have sufficient momentum to even make it into the tracker or the calorimeter, there is a tail in that distribution that goes up to the conversion electron momentum (Fig. 6). This background is defeated by the superb momentum resolution of the tracker, and in particular, the absence of high-side misreconstructions of the decay-in-orbit electron momentum (Fig. 9).

Other such backgrounds include radiative muon capture, $\mu^- \mathrm{Al} \rightarrow \gamma \nu_\mu \mathrm{Mg}$, where the gamma converts into an electron-positron pair with the electron carrying off most of the energy. This background is reduced by our choice of target: the daughter Mg nucleus is more massive than Al, reducing the endpoint energy of the electron to below the conversion electron energy. This, in concert with the excellent energy resolution of the tracker, reduces this background to a negligible

level.

Beam related backgrounds include electrons from muon decay-in-flight: $\mu^- \to e^- \nu_\mu \overline{\nu}_e$, pion decay-in-flight: $\pi^- \to e^- \overline{\nu}_e$, beam electrons that scatter in the stopping target, and radiative pion capture: $\pi^- \mathrm{Al} \to \gamma \mathrm{Mg}$, where the gamma converts asymmetrically into an electron-positron pair.[2] These are defeated by: requiring that the conversion electrons be significantly delayed with respect to the incident muon bunch time on the stopping target, hard cuts on the beam particle momentum, and the requirement that less than 10^{-10} of the incident protons on the production target come in the time period between the proton bunches. To reduce the number of particles in between the proton bunches, an extinction system has been fabricated that consists of a very fast switching dipole that deflects any such interbunch protons into a dump. To monitor its efficacy, an extinction monitor has been designed that measures the rate of such interbunch protons.

There are also anti-protons produced in the production target that make their way slowly through the transport solenoid, such that if they annihilated in the stopping target, could produce conversion-like electrons in the delayed live signal window. These are reduced to a negligible level by two thin aluminum windows: one at the beginning of the transport solenoid, the other at the center of the transport solenoid.

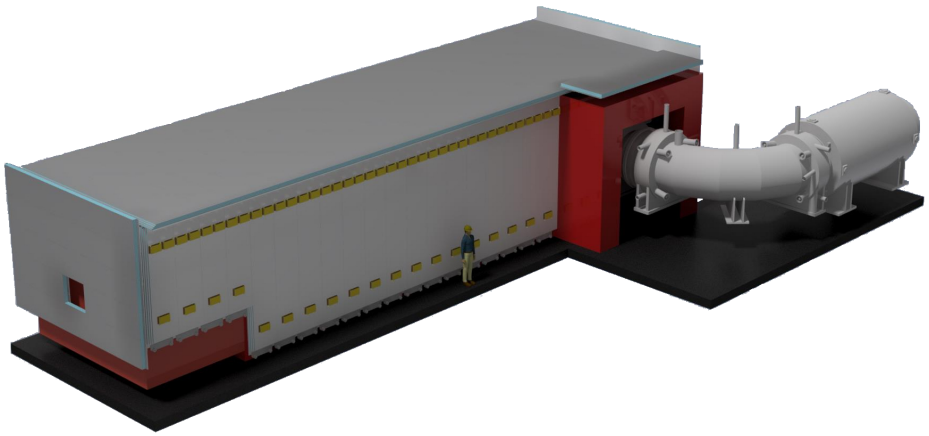

Figure 13: The cosmic ray veto detector surrounding the detector solenoid and half of the transport solenoid.

Cosmic rays can produce conversion-like electrons in the live signal window from muon decay-in-flight, neutron interactions, and muons mis-identified as conversion electrons. Such events are expected to appear at a rate of roughly one per day. To identify such events, a cosmic ray veto (CRV) detector has been fabricated that surrounds much of the apparatus (Fig. 13). The CRV consists of four layers of scintillator bars with embedded wavelength-shifting fibers, read out by silicon photomultipliers. A conversion-like electron in the signal region that comes in coincidence with a signal in the CRV is vetoed in the off-line analysis.

Figure 14 gives the relative sizes of the expected backgrounds, from a careful study of Run 1 backgrounds given in Ref. [6]. The total background is 0.11 ± 0.03 events. The largest background is produced from cosmic rays. The next largest is from muon decay-in-orbit. Backgrounds from radiative pion capture, radiative muon capture, decays in flight, and beam electrons are negligible.

[2] Approximately 1% of these events have a gamma energy greater than 105 MeV.

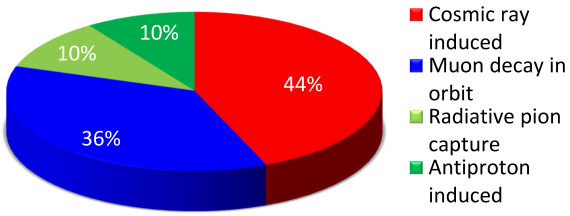

Figure 14: The fraction of the total background rate from the four largest contributors.

5. Expected Sensitivity

At the present time it is expected that there will be two runs of the experiment: an initial run of short duration followed by a longer run after a two-year shutdown to allow for the PIP-II upgrade of the Fermilab accelerator complex. The second run is expected to provide an order of magnitude increase in statistics from a more intense beam and a longer running period.

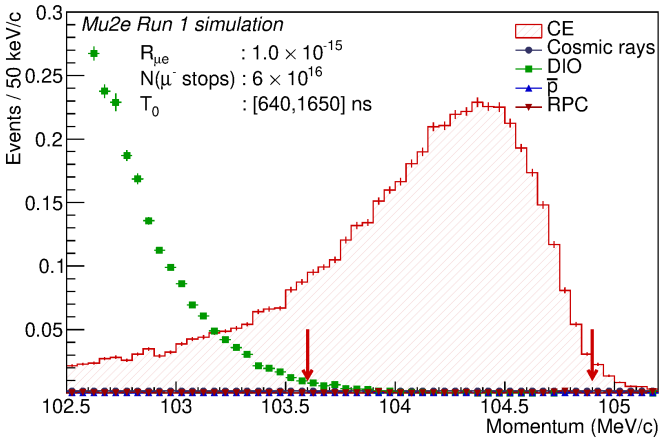

Figure 15: The signal region (between arrows) showing the major backgrounds and a conversion electron signal of $R_{\mu e} = 1 \times 10^{-15}$ [6].

The collaboration has carried out a detailed study of the anticipated Run 1 sensitivity and backgrounds [6]. The expected sensitivity for the ratio of the conversion process to the capture process is $R_{\mu e} = 1.2 \times 10^{-15}$ for a 5σ discovery, with a total expected background of 0.11 ± 0.03 events. In the absence of a signal, the expected upper limits is $R_{\mu e} < 6.2 \times 10^{-16}$ at 90% CL. This is a three order of magnitude improvement over the current limit set by the SINDRUM II experiment [7]. Similarly detailed studies have not yet been performed for Run II, but we expect to achieve and additional order of magnitude improvement in sensitivity.

6. Conclusions

The fabrication of the apparatus is over 90% complete. With first beam expected in 2026, and results from similar experiments in Europe and Japan expected by mid-decade, there is great anticipation that new physics may soon reveal itself through CLFV. If not, or if it does and there

is a need to reveal the exact nature of this new physics, the collaboration has proposed an upgrade, Mu2e-II, whose goal is another order of magnitude increase in sensitivity using the more intense PIP-II linac beam [8].

7. Acknowledgements

We are grateful for the vital contributions of the Fermilab staff and the technical staff of the participating institutions. This work was supported by the US Department of Energy; the Istituto Nazionale di Fisica Nucleare, Italy; the Science and Technology Facilities Council, UK; the Ministry of Education and Science, Russian Federation; the National Science Foundation, USA; the Thousand Talents Plan, China; the Helmholtz Association, Germany; and the EU Horizon 2020 Research and Innovation Program under the Marie Sklodowska-Curie Grant Agreement No.690835. This document was prepared by members of the Mu2e Collaboration using the resources of the Fermi National Accelerator Laboratory (Fermilab), a U.S. Department of Energy, Office of Science, HEP User Facility. Fermilab is managed by Fermi Research Alliance, LLC (FRA), acting under Contract No. DE-AC02-07CH11359.

References

[1] Altmannshofer et al., NPB 830, 17 (2010).

[2] E.P. Hincks and B. Pontecorvo, PR 73, 257 (1947).

[3] L. Bortoszek et al., *Mu2e Technical Design Report*, arXiv:1501.05241 (2015).

[4] R. Dzhilkibaev and V. Lobashev, Sov. J. Nucl. Phys. (1989) 49, 384–385.

[5] A. Czarnecki, X. Garcia i Tormo, W.J. Marciano, Phys. Rev. D 2011, 84.

[6] F. Abdi et al., Universe 9 (2023) 1,54.

[7] W. Bertl et al., Eur. Phys. J. C **47**, 337 (2006).

[8] K. Byrum et al., arXiv:2203.07569 (2022).